A Comprehensive Model of Single Particle Pulverized Coal Combustion Extended to Oxy-coal Conditions

Troy Holland and Thomas H. Fletcher*

350 CB

Chemical Engineering Department

Brigham Young University

Provo, UT, USA 84602

*Corresponding author,

email: tom_fletcher@byu.edu,

phone: 1-801-422-6236

Abstract

Oxy-fired coal combustion is a promising potential carbon capture technology. Predictive CFD simulations are valuable tools in evaluating and deploying oxy-fuel and other carbon capture technologies either as retrofit technologies or for new construction. However, accurate predictive simulations require physically realistic submodels with low computational requirements. In particular, comprehensive char oxidation and gasification models have been developed that describe multiple reaction and diffusion processes. This work extends a comprehensive char conversion code (CCK), which treats surface oxidation and gasification reactions as well as the processes such as film diffusion, pore diffusion, ash encapsulation, and annealing. In this work several submodels in the CCK code were updated with more realistic physics or otherwise extended to function in oxy-coal conditions. Improved submodels include the annealing model, the swelling model, the mode of burning parameter, and the kinetic model, as well as the addition of the Chemical Percolation Devolatilization (CPD) model. Results of the char combustion model are compared to oxy-coal data, and further compared to parallel data sets near conventional conditions. A potential method to apply the detailed code in CFD work is given.

Key Words: coal, char oxidation, oxy-fuel, kinetics, sensitivity analysis

Nomenclature

Parameter(s)	Description
A_c	The preexponential factor for computing the CO/CO_2 ratio
A_d	The preexponential factor in the thermal annealing reaction
A_p	Particle area (m^2)
$A_{R,1}$-$A_{R,8}$	The preexponential factor for 8 reactions and 2 reverse reactions. These come largely from correlations, and can be adjusted for specific data.
c_0	The number of stable bridges
c_{HR}	An NMR structure based swelling parameter
c_j	The j^{th} coefficient of the NMR correlations
C_p	The per mass heat capacity of the char particle J/kg/K
$d_{p,0}$	The initial particle diameter, in microns
E_A	The activation energy in the annealing reaction
E_c	The activation energy for computing the CO/CO_2 ratio in cal/mol
$E_{R,1}$-$E_{R,8}$	The activation energy for 8 reactions and 2 reverse reactions. These come largely from correlations, and can be adjusted for specific data.
f_i	The fraction of active sites in bin "i" in the thermal annealing model
HHR	Higher Heating Rate
HR	The initial heating rate of the raw coal particle (K/s)
k_i	The rate constant of reaction "i" in the particle
m_p	The mass of the char particle (kg)
M_δ	The average molecular weight of the side chains in a coal "monomer"
M_{cl}	The average molecular weight of an aromatic cluster in a coal "monomer"
N	The intrinsic order of R2 (formation of CO_2 by combustion). This defaults to unity, but can be adjusted to explore other kinetic regimes.
p_0	The fraction of intact bridges
P_i	The partial pressure of reactive gas "i" at the surface of the particle
$r_{p,i}$	The rate of reaction "i" in the particle
s_{min}	A proximate analysis based swelling parameter
s_{var}	An NMR structure based swelling parameter
T_g	The gas temperature (K)
T_p	The particle temperature (K)
T_s	The temperature of the surroundings for radiative heat transfer (K)
X_c	The percentage carbon from the ultimate analysis
α	The mode of burning parameter
$\Delta H_{rxn,i}$	The enthalpy of reaction "i" in the particle
ε_p	Particle emissivity
η	The effectiveness factor
Φ_i	The Thiele modulus
ψ	A random pore model parameter. This value has some uncertainty, and defaults to 4.6.

σ	Stefan-Boltzman constant or a parameter in the log normal distribution
$\sigma+1$	The coordination number
τ/f	A random pore model parameter. This value has some uncertainty, and defaults to 12.
Ω	The swelling coefficient ($d_p/d_{p,0}$)

1. Introduction

Coal-fired power plants have provided a substantial percentage of global electricity for decades, and current outlooks indicate that they will continue to do so for the foreseeable future. The high proportion of electrical power generation is matched by a correspondingly high proportion of CO_2 emissions. In order to meet regulatory targets for reduced emissions, carbon capture and sequestration techniques must be employed, and oxycoal combustion is a promising potential solution.

Oxycoal combustion has been reviewed thoroughly elsewhere,[1, 2] but in essence it consists of injecting high purity O_2 with the pulverized coal rather than the conventional air-fired method. To reduce the boiler temperatures to manageable levels, the flue gas is typically recycled, producing a combustion environment with high concentrations of CO_2, O_2, and (potentially) H_2O. The flue gas then contains very high concentrations of CO_2, and the CO_2 is thus relatively easy to capture.

While an oxycoal system simplifies carbon capture, it also radically changes the environment the coal particles experience. The new environment changes the O_2 diffusion rate, may cool the char particle via endothermic gasification, and may alter the overall char consumption rate due to gasification reactions.[3] These effects and others such as reduced flame temperature, delayed ignition, decreased acid gases, and increased gas emissivity can largely be ascribed to differences between CO_2 and N_2 (the respective diluents in oxycoal and air-fired pulverized coal systems).[1] The change in diluent gas induces several interrelated effects that alter the burnout time and radiative behavior of the system, so accurate CFD

predictions of oxycoal combustion require models that describe these phenomena. This work supports computational fluid dynamics (CFD) modeling of oxy-coal boilers either for the retrofit of existing boilers or the construction of new oxy-coal fired power plants by providing a detailed code that can predict the temperature and burnout profiles of coal particles in a hot, oxidative environment. The detailed model could also be used to train low computational cost, reduced-order models to accurately describe a specific scenario.

2. Experimental

To conduct a relevant comparison, the model was executed at conditions related to real-world application. Here, the most applicable conditions are the oxy-coal combustion environment, so experimental data from the literature were chosen for comparison at useful conditions. The experimental data also allowed the kinetic parameters to be calibrated. The model was then compared both to the calibration data and similar data not used in the calibration. The experimental data referenced here were collected by Shaddix and Molina[4] and Geier et al.[5] The reactor consists of a burner-stabilized flat flame, a quartz chimney for gas and particles to flow through, and a coal particle inlet in the center of the burner. The particle temperatures were measured with a 2-color pyrometry system and the diameters were measured by imaging of the particle emission. No burnout data from probe measurements were available from this data set. The coal particle flow rate was sufficiently low that particles did not affect each other or the bulk gas composition. The data were for two subbituminous coals (Black Thunder and North Antelope) and two high volatile bituminous coals (Utah Skyline and Pittsburgh seam (Bailey)) which were subjected to conditions of 14 or 16% H_2O, 12, 24, or 36% O_2, and the balance CO_2, at gas temperatures ranging from approximately 1400-1700 K. The proximate and ultimate analyses of the coals and a summary of experimental conditions are given in Table 1 and Table 2. The char particles were in the reactor for up to approximately 0.2 seconds (post devolatilization), and on the order of 1,000

particle data triplets of temperature, location, and diameter were collected for each condition. These data were used in a related sensitivity analysis of the Carbon Conversion Kinetics (CCK) model[6] to determine which model parameters were most sensitive at oxy-fuel conditions, and to target model updates and refinements. These updates were implemented, but it should be noted that the updates did not detract from the ability of the CCK code to predict char behavior in conventional oxidation and combustion scenarios. Instead, it extended the submodels to also capture intense oxy-fuel conditions.

Table 1 - Proximate and Ultimate Analysis of Coal Particles between 76 and 105 microns

Coal	Moisture (% AR)	Ash (% AR)	Volatiles (% AR)	C (% daf)	H (% daf)	O (% daf)*	N (% daf)	S (% daf)
Black Thunder	9.34	4.84	42.34	68.96	5.00	25.41	0.97	0.45
Utah Skyline	1.69	10.2	40.79	79.4	6.09	12.25	1.67	0.59
Pittsburgh	0.47	6.95	35.89	81.26	5.55	10.17	1.54	2.16
North Antelope	10.83	5.54	39.64	72.12	5.45	21.08	1.00	0.35

*by difference

Table 2 - Summary of Experiments for Char Particles between 53 and 125 microns

Coal	O_2 Mol %	CO_2 Mol %	H_2O Mol %	Peak Particle Temp. (K)	Peak Gas Temp. (K)
Black Thunder	12	74	14	1732	1741
	24	62	14	1919	1710
	36	50	14	2147	1726
Pittsburgh	12	74	14	1889	1741
	24	62	14	2077	1710
	36	50	14	2248	1726
Utah Skyline	12	72	16	1954	1697
	24	60	16	2181	1700
	36	48	16	2564	1714
North Antelope	12	72	16	1931	1697
	24	60	16	2108	1700
	36	48	16	2414	1714

Table 3 shows a summary of parallel experiments conducted with N_2 diluent rather than CO_2. These data were not used in the calibration of the CCK/oxy model, but they were collected under parallel conditions in the same apparatus, for the same coal, and with the same size cuts. It is of interest to determine whether kinetic parameters calibrated solely in conventional conditions can predict oxy-coal combustion data.

Table 3 - N_2 Parallel Experiments

Coal	O_2 Mol %	N_2 Mol %	H_2O Mol %	Peak Particle Temp. (K)	Peak Gas Temp. (K)
Black Thunder	12	74	14	1861	1677
	24	62	14	2128	1711
	36	50	14	2289	1753
Pittsburgh	12	74	14	1770	1677
	24	62	14	2154	1711
	36	50	14	2313	1753
Utah Skyline	12	72	16	2091	1690
	24	60	16	2325	1692
	36	48	16	2520	1712
North Antelope	12	72	16	2080	1690
	24	60	16	2357	1692
	36	48	16	2532	1712

3. Model Development

3.1. Model Summary

The CCK/oxy model is motivated by the inability of past comprehensive models to fit data taken in oxy-fuel conditions. This failure has been observed in previous work by Holland and Fletcher[7] and by McConnel and Sutherland.[8] While the present work was guided by a sensitivity analysis of the CCK model, that sensitivity analysis strongly implied that the most influential model parameters were the

same parameter subset in all cases, almost entirely independent of combustion conditions or coal type.[7] Though the sensitivity analysis used half of the same data cited in the experimental section, the sensitivity analysis only indicated which submodels were most influential. In the present work, those models are updated, based solely on recent research and literature observations, and completely independent of the char burnout data. Thus, this model was constructed to more precisely capture the physics of char burnout and not merely to fit the selected data set. The char burnout data influenced the model only in the final stage of kinetic parameter calibration. A complete list of parameters is given by Holland.[9] Figure 1 is a logic map of CCK/oxy execution, while Table 4 shows the main equations of the model. The model is currently configured for an entrained flow reactor (specifically the flat flame burner referenced in Section 2), so minor modifications may be necessary for other reactor types.

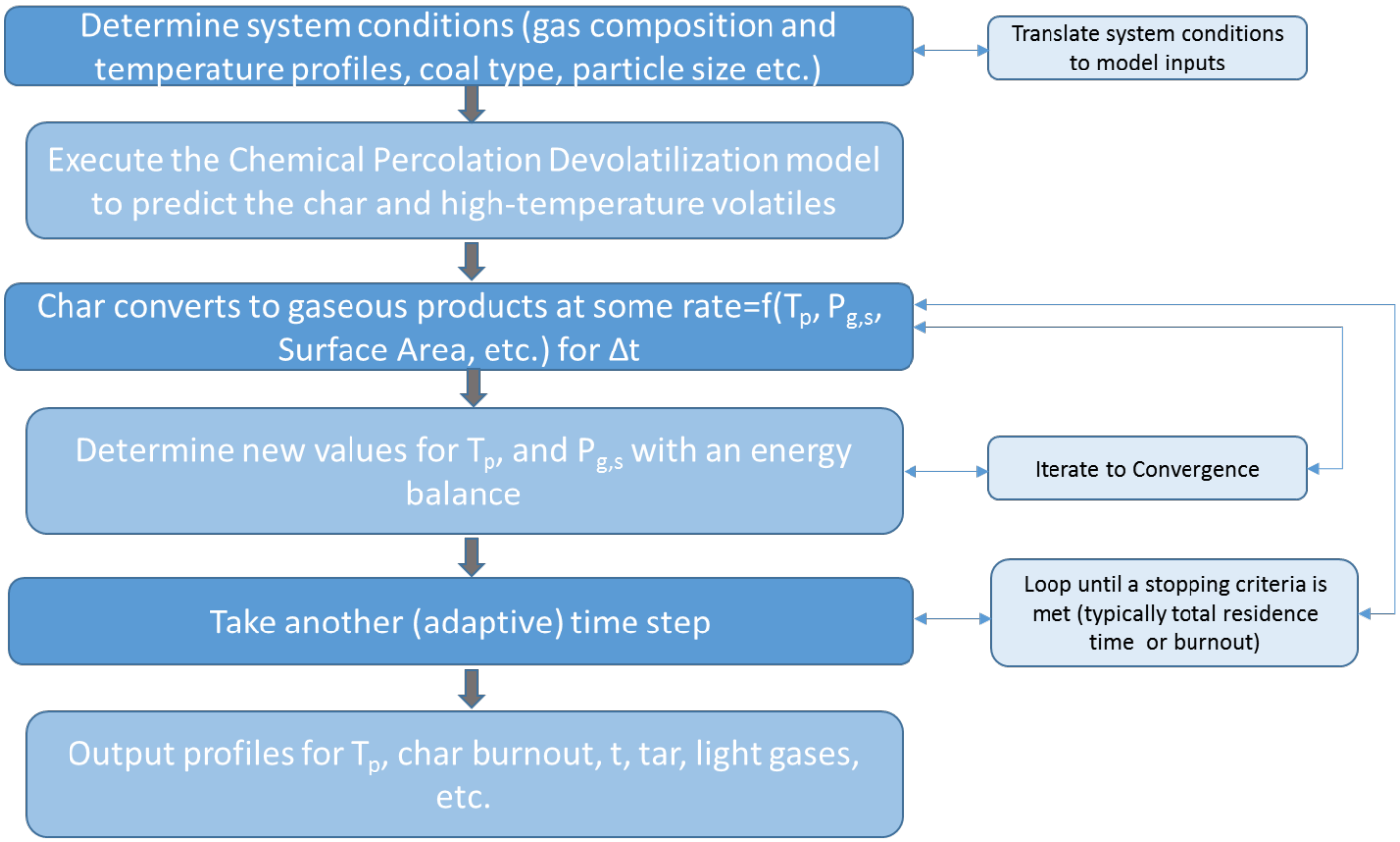

Figure 1 – Logic Map of CCK/Oxy Execution

Table 4 - CCK/oxy Submodels

Sub-Model Name	Model Form
Particle Energy Balance*	$m_p C_p \frac{dT_p}{dt} = hA_p(T_g - T_p) + \sigma\varepsilon_p A_p(T_s^4 - T_p^4) + \sum_i r_{p,i}\Delta H_{rxn,i}$ (1)
Surface Reactions [10]	$2C + O_2 \rightarrow C(O)_\alpha + CO$ $(R1)$ $C + O_2 + C(O)_\alpha \rightarrow C(O)_\alpha + CO_2$ $(R2)$ $C(O)_\alpha \rightarrow CO$ $(R3)$ $CO_2 + C \leftrightarrow C(O)_\beta + CO$ $(R4)$ $C(O)_\beta \rightarrow CO$ $(R5)$ $C + H_2O \leftrightarrow C(O)_\gamma + H_2$ $(R6)$ $C(O)_\gamma \rightarrow CO$ $(R7)$ $C + 2H_2 \rightarrow CH_4$ $(R8)$
Langmuir-Hinshelwood-type Reactions [10]	$R_{C-O_2} = \frac{k_1 k_2 P_{O_2}^2 + k_1 k_3 P_{O_2}}{k_1 P_{O_2} + \frac{k_3}{2}}$ (2) $R_{C-CO_2} = \frac{k_4 P_{CO_2}}{1 + \frac{k_4}{k_5}P_{CO_2} + \frac{k_{4r}}{k_5}P_{CO} + \frac{k_6}{k_7}P_{H_2O} + \frac{k_{6r}}{k_7}P_{H_2}}$ (3) $R_{C-H_2O} = \frac{k_8 P_{H_2O}}{1 + \frac{k_4}{k_5}P_{CO_2} + \frac{k_{4r}}{k_5}P_{CO} + \frac{k_6}{k_7}P_{H_2O} + \frac{k_{6r}}{k_7}P_{H_2}}$ (4)
Thermal Annealing [11†]	$\frac{df_i}{dt} = -f_i A_d \exp\left(\frac{E_A}{RT_p}\right)$ (5)
Thiele Modulus	$\phi_i = \frac{d_p}{2}\sqrt{\frac{\rho_C v_i (n_i + 1) R_{i,s}}{2 D_{eff,i} C_{i,s}}}$ (6)
Effectiveness Factor	$\eta_j = \frac{1}{\phi_j}\left[\coth\left(3\phi_j - \frac{1}{3\phi_j}\right)\right]$ (7)
Multi-component Diffusion	$D_{i,mix} = \frac{1 - y_i}{\sum_{j=1, j\neq i}^{Species} \frac{y_j}{D_{i,j}}}$ (8)

* All of the heat of reaction is applied to the char particle, and Eq. 13 dictates the ratio of CO to CO_2

† The annealing model is a complex set of statements to determine E_A and A_d. Details are given below.

Random Pore Model[12]	$\frac{A_p}{A_{p,0}} = (1-x) * \sqrt[2]{1-\psi * \ln(1-x)}$ (9)
High Heating Rate Particle Swelling[13]	$\frac{d}{d_0} = s_{var}\left(\frac{\dot{T}_{base}}{\dot{T}}\right)^{c_{HR}} + s_{min}$ (10)
Low Heating Rate Particle Swelling[13]	$\left(\frac{d}{d_0}\right)_{LHR} = m * \log(\dot{T}) + b$ (11)
Devolatilization Model	The CPD model is complex. Some detail is given below, and further details are referenced.
Gas Property Models[14, 15]	Polynomials from tabulated data used to calculate gas phase thermal conductivity and heat capacity as a function of temperature and molar composition.
Mode of Burning[16, 17]	$\frac{d\rho_p}{dt} = \frac{dm_p}{dt}\frac{\eta}{V_p}$ (12)
CO/CO_2 ratio[18, 19]	$\frac{CO}{CO_2} = A_c \exp(\frac{E_c}{R * T_p})$ (13)

3.2. Previous Models

Several char conversion models include complex submodels that attempt to capture the most important chemistry and transport effects of char conversion. The code used here is an extension of the Carbon Conversion Kinetics (CCK) code[10, 20] with numerous additions to make the code functional and accurate in the extremes of oxycoal combustion. These modifications include a more stable temperature solver with informed initial guess values that result in rapid convergence times, step-size independence, and successful model execution at extremely high temperature (appropriate for highly elevated O_2 concentrations) or high H_2O and CO_2 concentration environments. A number of key submodels were also revised or replaced to more nearly approximate the physics of heterogeneous char conversion. Predecessors of the CCK code include Carbon Burnout Kinetics - extended (CBK/E),[21] and Carbon Burnout Kinetics – gasification (CBK/G)[22] codes (which grew out of the Carbon Burnout Kinetics or CBK code[11]).

CBK/E utilizes a 3-step char oxidation reaction with O_2 (reaction equations R1-R3) first introduced by Hurt and Calo,[23] while CBK/G introduced a 5-step gasification model with CO_2, H_2O, and H_2 (R4-R5).

CCK combined these two equation sets into a single, 8-step mechanism theoretically capable of handling the common gasification species (optionally at high pressure) within a single model.[10] Note that in the 8-step mechanism shown in Table 4, the C(O) complexes in reactions R3, R5, and R7 represent distinct species with separate reactant pools, as denoted by the subscripts α, β, and γ. The above models successfully described the details of char conversion for oxidation, gasification, and pressurized gasification, but they were neither designed for, nor tested at the unusual gas compositions and combustion temperature found in oxy-coal combustion. Further details of the CCK and CBK-type models are available elsewhere.[10, 11, 20-22]

3.3. Practical Model Execution Considerations

The next several sub-sections outline the work done to improve the most influential submodels of the CCK/oxy code. While it is tempting (and often effective) to adjust some of the numerous uncertain parameters in the char combustion code until a desirable fit to data is obtained, this method of tuning to data results in a code that is often less predictive and less broadly applicable. Thus, with the goal of producing a combustion code with the widest possible applicability, the CCK/oxy model as a whole was not tuned to the specific data used here until the final optimization of the kinetic parameters. Instead, each submodel is in general compliance with char conversion theory and a subset of data related to the specific function of the submodel (i.e.; the swelling submodel was tuned to data that only related to swelling, etc.). The CCK/oxy model still contains several uncertain parameters related to such values as char tortuosity or ash grain size; since these values are generally unavailable for specific coals, default values are used.

Prior to revising submodels, several practical issues had to be resolved in code execution. These same issues are quite likely to arise in any attempt to modify a char combustion code from conventional to oxy-coal conditions, and are therefore worth mentioning briefly.

First, oxy-coal systems tend to have a higher O_2 concentration to compensate for the slower diffusivity of O_2 through CO_2 and the cooling effects of endothermic gasification reactions. The high O_2 concentrations can lead to very high local char combustion temperatures, and the high temperature, abundant O_2, and concentrated CO_2 and H_2O combine for an ambient environment that converts solid carbon very rapidly. Because char conversion codes are typically numerical solutions of sequential time steps, the reactant surface partial pressure is used throughout the time step, and the especially intense conditions of oxy-fuel are not likely to be fully grid-converged in models that functioned well at conventional conditions. The second issue is a direct consequence of the first; unrealistically fast carbon conversion leads to excessive temperature spikes that diverge rapidly from experimental data. The solution to both of these issues was an adaptive time step tied to the particle temperature change. In the initial particle heating phase, when gasification and combustion reactions are negligible, the particle is permitted to change temperature significantly in a single time step, but if the magnitude of change is too great, then the step is retaken with a smaller time step. In the current model, 10 K in a single time step is found to be more than sufficiently restrictive to ensure grid convergence in the cold region. When the particle is hot enough to react at a meaningful rate, the time step is instead tied to the ability of the particle to rapidly converge to a new temperature and surface reactant concentration via diffusion and the particle energy balance (which leads to much smaller time steps). Together, the adaptive time step was effective in maintaining grid convergence and reasonably rapid model execution.

The final practical code execution issue resulted from O_2, CO_2, and H_2O all becoming important reactants in the oxy-coal environment. The balance between exothermic oxidation and endothermic

gasification makes the energy balance difficult to converge even before attempting to match the model to data. More robust solver constraints and a relatively conservative and adaptive guess function for the new particle temperature ameliorated this issue, but there are still significant combinations of kinetic parameter space that lead to physically absurd results or outright model failure. It is impractical to search the entire kinetic parameter space as part of the optimization routine, but infeasible to put simple constraints on an irregularly shaped, high-dimensional kinetic parameter space. The details of the kinetics are discussed below, but the simple, practical solution was to explore the kinetic parameter space with a space-filling design. In this case, a Latin Hyper-cube design[24] was used, and an alternative pathway detected and reported non-physical parameter sets. This method was insufficient to wholly avoid physically infeasible space, but it did reveal the contours of several "valleys" of parameter space that contained local minima for an optimization objective function. By using these valleys as starting points for the final optimization, local minima were located with minimal intrusion into unphysical parameter space, and optimization routines became practical to execute.

3.4. Chemical Percolation Devolatilization Code

The chemical percolation devolatilization (CPD) model[25, 26] calculates the time-dependent release of volatiles as a function of coal type, heating rate, temperature, and pressure. The mechanism for thermal decomposition in the CPD model is directly related to the initial chemical structure, and the rates for cleavage of bonds between aromatic clusters are modeled. A Bethe lattice along with percolation lattice statistics is used to relate the number of cleaved bridges to the fraction of clusters that are not attached to the lattice. A flash calculation is used to relate vapor pressure to the amount of released tar vs. the amount of metaplast remaining in the particle. Crosslinking of metaplast to the char particle is also modeled.

The CPD code was recoded into a compatible format and linked to the CCK/oxy code to allow a complete prediction of the coal particle in a given set of circumstances. With a single set of inputs to describe the ambient environment, CCK/oxy produces a prediction that tracks the coal particle from raw coal, through initial heating and devolatilization, and throughout gasification and complete burnout. Because the thermal annealing kinetics are quite rapid, it is generally thought to be sufficient to execute the devolatilization code in the absence of annealing, and then to allow annealing to begin at the same time as combustion (despite most annealing actually taking place during the devolatilization phase). This is valid only if the consumption of char is negligible during devolatilization, *and* if the annealing of the char "catches up" before significant amounts of char are converted. Both assumptions are reasonable in typical combustion regimes, but this assumption was tested here by intertwining the annealing with the devolatilization model and the char conversion model. No significant difference was manifested when allowing annealing and devolatilization to occur sequentially vs. the more physically appropriate (but computationally onerous) concurrent computation of devolatilization and the annealing submodels.

The CPD code and three other submodels employed in CCK/oxy (the kinetics, swelling, and annealing submodels) require information from the ^{13}C Nuclear Magnetic Resonance Imaging (NMR) parameters. These parameters contain important structural information about the coal, but they are not generally available for most coals. Therefore, to maintain a high degree of applicability, the NMR parameter correlations reported by Genetti et al.[27] were used. These nonlinear correlations were developed to predict the NMR parameters of any coal based only on the widely available proximate and ultimate analysis, and are described briefly below, with more detail available elsewhere[27, 28].

3.5. The Mode of Burning Parameter

Porous fuel particles are typically considered to gasify in one of three regimes or zones. They may be entirely kinetic limited, entirely film diffusion limited, or exhibit a mixture of internal diffusion and kinetic limitations. Kinetic limitations imply a relatively cool particle, which is not the case of coal char at practical combustion conditions. However, since gasification reactions with CO_2 and H_2O have enhanced importance in the oxy-fuel scenario, and because the associated activation energies are much higher than that of combustion in O_2, kinetic limitations may well be expected to have a significant impact on char conversion. Because the three regimes have very different implications for char consumption, the concept of a mode of burning parameter, α, has historically been used to balance the shrinking diameter with the decrease in density in accordance with the char conversion regime (film diffusion limited, kinetically limited, or somewhere in between).[29-31] An equation relating mode of burning, mass, and diameter is show below (Equation 17), with α=0 indicative of constant density and thus a complete film diffusion limitation, while α=1 implies constant diameter with kinetic limitation. In conventional, air-fired char combustion an α value of 0.2 is recommended.[11, 32]

$$\frac{\rho}{\rho_0} = \left(\frac{m}{m_0}\right)^{\alpha} \qquad (14)$$

In the construction of the CCK model, it was intended that the model should be run at either combustion conditions or gasification conditions, while oxy-coal combines the high temperature and O_2 conditions of combustion with the high CO_2 (and sometimes H_2O) concentration of gasification. Thus, while the CCK code could match data well with a simple heuristic to determine α, the CCK/oxy model is a significantly more complicated situation. Moreover, oxy-coal might have a very wide range of O_2 concentrations, depending on the specific application, which in turn leads to a broad range for particle temperature that heavily influences the value of α relevant to gasification. Finally, global coal combustion models (and CCK) simply designate a mode of burning as a constant for a given instance, but in reality the balance between diameter loss and density decrease is

far from static during char particle burnout. Given the sensitivity of the CCK model to α[7], it was necessary to significantly improve the mode of burning implementation in CCK/oxy using a variation on a method derived and applied by Haugen et al.[16, 17] This method is derived in detail elsewhere,[17] but the key results are shown in Equations 15 and 16. The results below were obtained using the Thiele modulus relevant to a first-order, irreversible reaction at steady state, and also assumed a relatively large value of the Thiele modulus such that the effectiveness factor could be approximated by Equation 17. In reality, the order of the combustion reaction is a matter of controversy that depends both on how the kinetic system of equations is framed and on the temperature regime; also the effectiveness factor may not be small for gasification reactions. However, the method shown in the equations below is considerably superior to a single, fixed value of α, and establishes a conceptually sound relation between the changes in particle diameter and density for the reactive regime of the oxidative gasses.

$$\frac{dr_p}{dt} = \frac{dm_p}{dt}\frac{1-\eta}{4\pi r_p^2 \rho_p} \tag{15}$$

$$\frac{d\rho_p}{dt} = \frac{dm_p}{dt}\frac{\eta}{V_p} \tag{16}$$

$$\eta \approx \frac{3}{\phi} \tag{17}$$

In the case of a near-zero effectiveness factor, the particle is diffusion limited and the radius change represents the entire mass loss of the particle, while the density is essentially constant. In the case of η=1, the char particle is kinetically limited, and the diameter is essentially constant. These equations are exactly true under the assumptions used in the derivation (first-order, irreversible kinetics modeled by the Thiele modulus at steady state, and a small effectiveness factor). In CCK/oxy, the effectiveness factors for reaction with O_2, CO_2, and H_2O are computed at each time step, and then they are weighted according to the fraction of carbon consumption that is due to each reaction pathway. The weighted effectiveness factor for a given time step is used to compute the change in density for that time step, and the change in density is then used in conjunction with the computed conversion of carbon (from the kinetic and gas diffusion submodels) to compute the diameter decrease for the

time step. This second step is done because, as mentioned above, some of the assumption in the derivation of Equations 15 and 16 are only approximations in the reality of char combustion. Thus, Equation 15 for the change in radius is superseded by enforcing the law of conservation of mass, which corrects for the inconsistency introduced by the approximations of the derivation.

3.6. Coal Particle Swelling Model

The swelling submodel employed in the CCK model is overly simplistic. The most advanced swelling models attempt to capture the physics of bubble formation,[33-35] but are impractical because they are computationally expensive, complicated to implement, and may not be applicable to a wide range of coals. Most importantly, until recently,[34, 35] these swelling models do not follow the observed swelling trends at the extremely high heating rates (10^4-10^6 K/s) relevant to practical coal combustion systems.[36] This is true of all swelling models that neglect the functional dependence on heating rate, and is presumably because the extreme heating rates drive the volatiles from the particle very rapidly.[21, 37] The rapid loss of volatiles leads to a very short time-frame for bubble formation, and when the rate of bubble growth exceeds the rate of metaplast relaxation, the bubbles "pop" leading to an entirely different swelling regime.[38]

The swelling model implemented in CCK/oxy incorporates information about the coal structure and type as well as heating rate dependence, with the structural parameters predicted from the NMR correlations mentioned previously. Both the coal type and heating rate heavily impact the swelling behavior.[37] The newly implemental model was developed by Shurtz et al. [13, 20] and a brief description of equations and applicability is given below, with details of the swelling model development given elsewhere.[13, 20] The swelling ratio is given by Equation 18, where s_{var}, c_{HR}, and s_{min}, are described by the correlations in Table 5, and $\dot{T}$ is the maximum heating rate that the particle experiences during the heat-up and swelling process (in K/s, as estimated via the transient particle energy balance). This maximum rate occurs at initial heating, when the cold particle experiences the greatest temperature

gradient with its surroundings. Table 5 (reproduced from Shurtz et al.[13]) gives the value for other variables of interest, as well as their range of applicability. Here σ+1 indicates the coordination number, M_δ refers to the average molecular weight of the side chains, HHR applies to the high heating rate regime, and FC_{ASTM} and A_{ASTM} are the American Society for Testing and Materials (ASTM) values for ash and fixed carbon content, respectively. $\dot{T}_{base}$ is set at 5.8×10^4 K/s.

$$\left(\frac{d}{d_0}\right)_{HHR} = s_{var}\left(\frac{\dot{T}_{base}}{\dot{T}}\right)^{c_{HR}} + s_{min} \tag{18}$$

$$s_{min} = (FC_{ASTM} + A_{ASTM})^{1/3} \tag{19}$$

Table 5 - High Heating Rate Swelling Model Parameter Correlations

Correlation	Applicable Range
$s_{var} = 1.69\frac{\sigma+1}{M_\delta} - 0.0309$	$0.018 \le \frac{\sigma+1}{M_\delta} < 0.207$
$s_{var} = -3.37\frac{\sigma+1}{M_\delta} + 1.01$	$0.207 \le \frac{\sigma+1}{M_\delta} \le 0.301$
$s_{var} = 0$	$\frac{\sigma+1}{M_\delta} < 0.018 \; or \; \frac{\sigma+1}{M_\delta} > 0.301$
$c_{HR} = -191\left(\frac{\sigma+1}{M_\delta}\right)^2 + 68.9\frac{\sigma+1}{M_\delta} - 5.16$	$0.106 < \frac{\sigma+1}{M_\delta} < 0.254$
$c_{HR} = 0$	$\frac{\sigma+1}{M_\delta} < 0.106 \; or \; \frac{\sigma+1}{M_\delta} > 0.254$

The preceding equations and parameters introduce the vital elements of heating rate and coal structure into the coal particle swelling model. Coal structure in particular is introduced via correlations with the NMR parameters mentioned previously, and allows for superior correlation than the less informative parameters of the proximate and ultimate analysis used previously. Equations 18 and 19 are intended for maximum heating rates of at least $8.3x10^3$ K/s, and have been shown to fit data taken at relevant heating rates and atmospheric pressure.[13] The CCK/oxy implementation of the swelling model also incorporates a plugin for adding in the influence of high-pressure on swelling (also developed by Shurtz et al. and detailed elsewhere[10]). For lower heating rates, Shurtz et al. [13] developed a piecewise correlation. The details are not relevant to typical combustion modeling, so, while CCK/oxy contains the low heating rate correlation, the details are not included here.

3.7. Thermal Annealing

The thermal annealing model encompasses the changes in raw coal due to both preparation conditions and activity loss during burnout. The initial chemical and physical changes during devolatilization are by far the most impactful, but in the intense heating conditions typical of industrial coal combustion, both sources of thermally induced changes to coal reactivity may occur on roughly the same time-scale, making it impossible to effectively separate the two effects. An extended annealing model that addresses both annealing effects is developed and discussed in detail elsewhere.[9] The results of the annealing model were incorporated in this work in Equations 20-25. Briefly, this annealing model differs from previous models used in comprehensive char conversion codes in that it accounts for both the rates of various annealing kinetic pathways *and* the changes to those pathways due to coal type, heating rate, and peak particle temperature. For example, if a given coal is heated at 10 K/min in a thermogravimetric analysis (TGA) device, the total volatile yield may be considerably less than if the same particle is heated at 10^5 K/s in a flat flame burner. The volatiles that are not released at low heating rate instead

cross-link back into the coal structure, giving the char particle a different chemistry, and altering not only the rate of annealing, but also the annealing pathways available based on the heating rate of char preparation. Alternatively, annealing experiments may commonly heat a char particle rapidly to approximately 1300 K. This temperature is often insufficient to melt the inorganic ash in a char particle, and molten inorganic ash loses all catalytic activity, while inorganic crystals may have catalytic activity for both carbon conversion and carbon crystal rearrangement reactions; thus peak particle temperature can also impact both the extent of annealing and the available annealing pathways.

In the equations below, f is the fraction of active sites in bin "i," k is the preexponential factor for the rate of active site loss (constant for all bins), and $E_{A,i}$ is the activation energy from the i^{th} bin of the log normal distributed activation energy profile. The parameters "a" through "d" were optimized from a large collection of data tabulated elsewhere, while σ and μ are parameters for the log normal distribution, and p_0 is the fraction of intact bridges from the NMR structural parameter correlations. Finally, there are also two truncation factors that transform the log normal activation energy distribution into a bimodal distribution to represent the two main sets of annealing reaction pathways (devolatilization and thermal deactivation). Parameter values for this work are shown in Table 6.

The variable "f" merits slightly more explanation. Because the total number of active sites is unknowable, the total number of sites assigned to a given bin is equally unknowable. Fortunately, the annealing model is only needed to calculate the rate of active site loss relative to the original reactivity of the particle, so the number of sites in each bin may be normalized by the unknown original number of sites. Thus, in theory, $f_i=N_i/N_0$ (where N is the number of active sites), but in practice f_i is some value between 0 and 1, and the values of all f's (initially) sum to 1. Once the number of bins is set, the initial values for f_i are set to conform to a probability density function (PDF), and in this case a discretized, truncated log-normal PDF was found to be appropriate. The sum of the f_i's at any time becomes the

fraction of sites that are active, and hence becomes a multiplier in the reaction rate expression that starts at 1.0 and decreases with time.

$$\frac{df_i}{dt} = -A_d * exp\left(\frac{-E_{A_{anneal},i}}{RT}\right) * f_i \quad (20)$$

$$PDF(E_{A_{anneal},i}) = \frac{1}{E_{A_{anneal},i} * \sigma} \exp\left(-\frac{1}{2}\left(\frac{ln\left(E_{A_{anneal},i}/\mu\right)}{\sigma}\right)^2\right) \quad (21)$$

$$\mu = a * p_0 + b * T_{peak} + c \quad (22)$$

$$\sigma = \frac{d}{p_0} \quad (23)$$

$$A_d = \frac{p_0 * k_0}{\ln(10^4)} \qquad for\ HR \geq 10^4 \quad (24)$$

$$A_d = \frac{p_0 * k_0}{\ln(\mathrm{HR} + 2.7)} \qquad for\ HR < 10^4 \quad (25)$$

Table 6 – Annealing Parameter Values

Parameter	Value
k_0	$1.398*10^{12}$ s^{-1}
a	0.356 ln(kcal/mol)
b	$3.65*10^{-4}$ ln(kcal/mol)
c	1.531 ln(kcal/mol)
d	0.679 ln(kcal/mol)

3.8. Gasification and Oxidation Kinetic Equations and Parameters

The reaction steps R1-R8 each have an associated activation energy and preexponential factor for a total of 20 kinetic parameters (including two reverse reactions). This kinetic scheme was given in the CCK

model as a combination of the combustion kinetic scheme from CBK/E and the 5 gasification reactions from CBK/G. A system of only eight reactions is an extremely simplistic skeletal mechanism attempting to capture the most prominent collective effects of innumerable unknown coal combustion reactions, but it has nevertheless proven sufficiently flexible to fit a broad sampling of combustion and gasification data.[10, 22] In fact, the kinetic system generally has more than enough free parameters, and the data of a given combustion scenario are typically insufficient to effectively optimize 20 parameters. This was recognized in the introduction of CBK/G, and it is typically sufficient to fit only the four kinetic parameters involved in R3 and R7 (k_3, E_3, k_7, and E_7), where R3 is the principle combustion reaction and R7 is the principle gasification reaction. The rest of the kinetic parameters are either fixed at nominal values or tied to the kinetic parameters of R3 and R7 via correlations developed with CBK/G.[22]

After the preceding submodels were updated or added to the CCK/oxy model, the kinetic parameters were optimized. It is important to note that this optimization is not a fit of the kinetic parameters as is typically observed with a single, linearized reaction equation fit to a set of rate data. Instead, the entire parameter space is given bounds and, optionally, both linear and nonlinear constraints. An initial guess value was provided for each parameter, and the optimization algorithm fmincon (from the MATLAB Optimization Toolbox) explored the constrained parameter space to minimize the error of an objective function.

4. Results and Discussion

Model development essentially consisted of two steps. First, numerical and model execution issues from CCK that caused the CCK/oxy model to fail in the extremes of the oxy-coal environment were eliminated. Second, the most sensitive submodels were replaced with updated, more physically realistic submodels. Because the models are simply more refined, rather than specific to the oxy-coal

environment, improvements realized by the updated model are valid in gasification, air-fired, and oxy-coal conditions. This section compares the relatively limited oxy-coal data to the CCK/oxy model, after optimizing the kinetic parameters as described in Section 3.8.

In considering the results, note that the data have a very wide range of particle temperature values; at any given observation height and particle diameter the particle temperatures range on the order of ±150 K from the mean. However, the trends in the data may be due to more than merely noisy data, and in fact the data are not actually "noisy" in the traditional sense. Instead, the data indicate the actual temperature variation due to particle-to-particle variation in ash content and/or maceral character (variation due to measurement uncertainty may be on the order of ±25 K).[32, 39]

4.1. Particle Diameter Determination

As shown in the experimental section, the data are for four different coals burned at each of three conditions. The data collection system was able to measure the diameter and temperature of individual particles at pre-determined heights in the burner. Table 7 and Table 8 show the mean of particle diameter and temperature for each height for two of the coals, but the other two coals reported only the average temperature data, which are shown in Table 9 and Table 10. The more complete data for Utah Skyline and North Antelope coals have several implications for the behavior of the experiment. Most importantly, the cohort of particles observed at a given height is NOT the same cohort as observed at lower burner heights. The burner height is adjusted between experiments, so the individual particles are different specific particles, but more importantly, the average characteristics of an observed particle change based on observation height. This is because of at least four competing effects that alter which particle cohort is most likely to be "seen" by the detector system:

1. The detection method relies on the light emitted by burning particles, so some particles simply are not detected. A particle is most likely to be detected if it is large and hot (and thus emitting a relatively large quantity of light).
2. Small particles tend to burn hotter than larger particles, but have less surface area and thus emit less total light than a larger particle of the same temperature.
3. As particles burn, the smaller particles reach near extinction relatively quickly, and without the heat of reaction the particle temperature drops below the gas temperature due to radiative losses. These non-burning or slow-burning particles then become invisible to the detection system. This increases the average diameter of the detected particles and decreases the number of particles detected. This effect is especially important for the very small particles that are below the nominal size cut (either from fragmentation or from imperfect sieving).
4. Large particles take longer to burn out into the undetectable range because they have both greater mass and a larger surface area to emit light. However, these initially large particles persist into later residence times and decrease in diameter during burnout, which decreases the average diameter of the detected particles.

Table 7 - Utah Skyline Data Summary

12% O_2						
Height (cm)	7.62	8.89	10.16	12.70		
Avg. D_p (μm)	106	102	96	98		
Avg. T_p (K)	1864	1857	1810	1815		
Number of Points	231	184	1078	198		
24% O_2						
Height (cm)	5.08	6.35	7.62	10.16	11.43	12.70
Avg. D_p (μm)	96	97	102	103	106	107
Avg. T_p (K)	2092	2088	2071	2049	2038	2013
Number of Points	195	233	214	180	195	100
36% O_2						
Height (cm)	6.35	7.62	8.89	10.16	11.43	12.70
Avg. D_p (μm)	111	120	119	124	123	122

Avg. T_p (K)	2290	2272	2256	2239	2219	2180
Number of Points	859	295	201	162	75	29

Table 8 - North Antelope Data Summary

12% O_2										
Height (cm)	7.62	8.89	10.16	11.43	12.70	13.97	15.24	16.51	17.78	19.05
Avg. D_p (µm)	86	89	88	88	91	86	96	96	94	103
Avg. T_p (K)	1851	1853	1873	1867	1870	1859	1876	1854	1860	1826
Number of Points	176	149	131	151	100	59	54	52	31	19
24% O_2										
Height (cm)	5.08	6.35	7.62	8.89	10.16					
Avg. D_p (µm)	92	96	96	97	100					
Avg. T_p (K)	2038	2054	2059	2077	2093					
Number of Points	191	211	293	129	37					
36% O_2										
Height (cm)	5.08	6.35	7.62	8.89	10.16					
Avg. D_p (µm)	100	106	110	96	92					
Avg. T_p (K)	2294	2323	2348	2363	2370					
Number of Points	200	200	157	105	23					

Table 9 - Black Thunder Data Summary

12% O_2								
Height (cm)	5.08	5.715	6.35	7.62	10.16	15.24	20.32	25.40
Avg. T_p (K)	1703	1708	1726	1732	1725	1715	1718	1690
24% O_2								
Height (cm)	4.45	5.08	5.715	6.35	7.62	10.16	12.70	
Avg. T_p (K)	1837	1894	1913	1914	1919	1879	1859	
36% O_2								
Height (cm)	3.18	3.81	4.45	5.08	7.62	10.16		
Avg. T_p (K)	2038	2052	2103	2147	2135	2072		

Table 10 - Pittsburgh 8 Data Summary

12% O_2							
Height (cm)	5.08	5.715	6.35	7.00	7.62	8.89	10.16
Avg. T_p (K)	1822	1824	1872	1855	1873	1889	1898
24% O_2							
Height (cm)	5.08	5.715	6.35	7.62	8.89	10.16	
Avg. T_p (K)	2037	2006	2054	2066	2077	2067	

36% O_2									
Height (cm)	3.18	3.81	4.45	5.08	5.715	6.35	7.62	8.89	10.16
Avg. T_p (K)	2028	2179	2207	2242	2248	2237	2245	2238	2186

Bearing the above effects in mind, it is not easy to immediately apply simple trends to the data, but some approximations are certainly necessary to input a more accurate particle size into the CCK/oxy model so that the comparison between data and model is legitimate. One obvious trend is the change in observed particle diameter between conditions. In general, more intense conditions have a larger average **observed** particle diameter, most likely because the high O_2 concentration rapidly consumes the smallest particles, and leaves a higher fraction of larger particles. Failure to account for these trends in coal particle diameter with burner height and O_2 condition leads to the inability of a model to match all of the data (i.e., if the model fits for the 12% O_2 environment, it won't fit for the 36% and vice versa).

The data clearly necessitate that different initial diameters be allowed for comparison with data from each measurement height. In general, the profiles of initial particle diameter and observation height (shown in Table 11) are taken from the diameter profiles of the observed data (in the case of North Antelope and Utah Skyline), or extrapolated from the North Antelope and Utah Skyline diameter profiles (in the case of Black Thunder and Pittsburgh 8). The extrapolation of North Antelope and Utah Skyline diameter profiles onto Black Thunder and Pittsburgh 8 (respectively) is necessary because the diameter profiles are not reported, but it is done on the frankly tenuous grounds that Black Thunder and North Antelope coals are both subbituminous while Pittsburgh 8 and Utah Skyline are both high-volatile bituminous coals. The resulting model/data fits are surprisingly good, but it must be emphasized that the Pittsburgh 8 and Black Thunder diameter profiles are extrapolations. It should also be emphasized that the diameter profiles are determined from the available data, and then the data are fit by adjusting **only**

the kinetic parameters. Thus, the coal particle diameter is somewhat uncertain, but it is NOT a free parameter, and it is not adjusted to get the "correct" fit.

The **observed** diameters during late-burnout are smaller than their initial value because the particles have decreased somewhat in size during burnout. The CCK/oxy model accepts the initial diameter as an input, and then predicts the diameter, temperature, and mass change of the particle throughout burnout. Therefore, where there is evidence that the observed diameter has decreased from the initial value (i.e., at later burnout times), this diameter change should be taken into account. The initial diameter is estimated from the observed diameter when modeling the late burnout data. It should be noted however, that while the profiles are reasonable given the size cut, predicted swelling, and diameter loss due to burn out, the late-burnout diameters are a slight extrapolation. The specific profiles of each coal have a few points worth noting:

1. The extrapolated profile for Black Thunder and Pittsburgh 8 were simply set at a lower bound of 90 and 95 μm respectively. Those coals were observed at much lower heights than the North Antelope and Utah Skyline coals, but, given the particle size cut, it is unreasonable that the average particle diameter would continue to follow a sharp downward trend at low observation heights.
2. In general, the North Antelope profiles are directly from the data with small increases of between 2 and 6 μm added to the initial diameter for data obtained at locations after the diameter data are observed to "peak." This peak indicates that the largest mean diameter has been reached from the effect of smaller particles burning out. Following the peak, the diameter decreases as diameter loss due to char conversion becomes the more prominent effect. This causes the mean diameter to gradually decrease or not increase as sharply as would otherwise be expected, and to get a closer estimate of the mean **initial** diameter for the observed late-burnout particles, it is

necessary to estimate the diameter loss. In the last two points of the 36% O_2 condition, the mean particle size dropped quite substantially because of the rapid burnout of the intense condition. Here, 15 microns were added, to bring the value approximately to the peak observed size; given that, generally, the largest particles will survive to late burnout, it is thought that the peak value is as good an estimate as can be made for late burnout particles.

3. The Pittsburgh 8 coal diameters are a rounded extrapolation from Utah Skyline diameter data. Also, the 12% O_2 condition in Utah Skyline is too narrow and noisy to be overly informative, so there was no justification for extrapolating a particular profile to Pittsburgh 8. Instead, the Pittsburgh 8 12% O_2 input was fixed at a rounded mean of the extrapolation (98 microns).
4. The Utah Skyline coal 12% O_2 environment is an anomaly in that the data begin with a relatively high diameter and then exhibit marked decreases in both diameter and particle temperature. Upon close examination of the complete set of relevant data (rather than just average values), it seems likely that fragmentation is the cause of this unusual behavior. The first two observation heights in the 12% O_2 environment have a relatively high proportion of large particles. However, at the third observation height (10.16 cm), the data show a significant increase in very small particles when the opposite trend is expected and observed in the remaining data. Specifically, the second observation height has nearly six times as large a proportion of very large (>180 μm) particles over the third observation height. Additionally, the second observation height has a seven-fold higher proportion of relatively hot particles (>1900 K), while the third observation shows a substantial increase of small, cold particles and a five-fold increase in total particles observed.
5. Like North Antelope, the Utah Skyline particle diameter in 36% O_2 is observed to peak and then decrease, so the original diameter of the cohort is crudely estimated to be between 4 and 8

microns higher than the observed diameter, based on the amount of post-peak decrease and the range of observed diameters.

Table 11 - Multiple Diameter Profiles

Coal Type	Black Thunder			North Antelope			Pittsburgh 8			Utah Skyline		
O_2 %	12	24	36	12	24	36	12	24	36	12	24	36
Height (cm)	Diameter (µm)			Diameter(µm)			Diameter (µm)			Diameter		
3.18			90						95			
3.81			90						95			
4.45		90	90						100			
5.08	90	90	90		92	100	98	95	105		96	
5.72	90	90					98	98	110			
6.35	90	90			96	106	98	98	110		97	111
7.00							98					
7.62	90		105	86	96	110	98	100	120	106	102	120
8.89				89	101	111	98	100	120	103		119
10.16	95	105	115	87	106	106	98	105	125	101	107	124
11.43				88							112	127
12.70		115		91						103	115	128
13.97				85								
15.24	105			96								
16.51				98								
17.78				97								
19.05				107								
20.32	105											
25.40	115											

4.2. Model/Data Fit

The results of fitting the revised CCK/oxy model to the Shaddix data are shown in Figure 2 and

Table 12. In this figure, the kinetic parameters are constant for any given coal, and the initial particle diameter is input into the CCK/oxy model. The model then predicts a temperature vs height profile, which is plotted from initial heat up (starting at 300 K), but truncated before complete burnout at the relevant burner height. The truncation improves graph readability, but it should be noted that the model appropriately predicts a late burnout drop in temperature. The mean absolute error values are on the order of the noise due to measurement error (±25 K). Systematic bias is nearly absent, and maximum errors fall in the expected range of measurement error, with two notable exceptions. First, the Pittsburgh 8 coal has an enormous maximum error (see Table 14) that is introducing a skew into the entire data set, especially in the 36% O_2 environment. (note that though the error is large, a diameter change of only a few microns has a very profound impact on the earliest observed particles because they are still in a very rapid heating phase). The error is because the extrapolation of coal diameter to the very low observation heights for the Pittsburgh 8 data appears to be incorrect. In the extrapolation, the 36% O_2 Pittsburgh 8 data were assigned diameters as low as 95 microns, because the observations began much earlier than Utah Skyline (where the lowest diameter was observed to be 111 microns). By changing the Pittsburgh 8 early burnout diameter values to 105 microns (still in-line with the known early burnout values at the Utah Skyline 36% O_2 condition), the mean absolute error was reduced to 36 K and the maximum error decreased to 65 K even without reoptimization. The sum squared error also decreased by more than 50% (also without reoptimization), because the single point in question contained more error than the sum of the entire data sets at all three O_2 conditions. Because of the dominant weight of that one point introducing a skew in the optimization objective function, reoptimization removed the skew and reduced the mean and maximum absolute errors in the 36% O_2 Pittsburgh 8 data to 21 and 42 K respectively, effectively eliminating one of the two remaining sources of notable bias. This is not shown in the plot, and is not reflected in the error tables because the updated result depends on an uncertain inference

based on post-optimization analysis. It seems likely that the extrapolation of the Pittsburgh 8 early burnout 36% O_2 condition was a few microns off, because a small change in the extrapolation makes all of the Pittsburgh 8 data self-consistent, but the actual cause of error is unknown.

The second largest maximum error coincides, as expected, with the other noteworthy bias. The 24% O_2 environment for Utah Skyline coal has a bias from one of several possible sources: bias in model prediction due to imperfect submodels, inappropriate extrapolation for the initial diameter inputs, a skew in the data etc. The extrapolation of the diameter data seems the mostly likely culprit, and it must be emphasized that **all** of the diameter profiles are, to some degree, an extrapolation. However, the extrapolation is quite reasonable to within a few microns given the data trends, and since the profiles were set prior to optimization, not adjusted post-optimization to match the CCK/oxy model, it is likely that any set of parameters following the observed trends in the data would be able to obtain an excellentfit with slightly different kinetic parameters. Thus, the data trends are important, but the actual diameter values only need to be correct to within a few microns.

This last observation highlights a potential difficulty in applying the CCK/oxy model. Frequently, coal particle burnout is determined by collecting a sample of partially burned char and measuring the level of conversion. Such an approach does not suffer from the weakness of observing only progressively more truncated portions of the total particle feed. However, data such as those used in the present work, represent only a portion of an unknown feed distribution. Thus, while the predictions and data show excellent agreement, and the CCK/oxy model is expected to perform well for the entire particle distribution, only a portion of the distribution is available for direct comparison and validation. A solution to this problem for Computational Fluid Dynamics (CFD) applications is addressed in greater detail in Section 5, but in general, the data here imply that nearly the entire particle distribution is “seen” in the 12% O_2 case, and hence one form of validation might be to extrapolate from the 12% O_2 case.

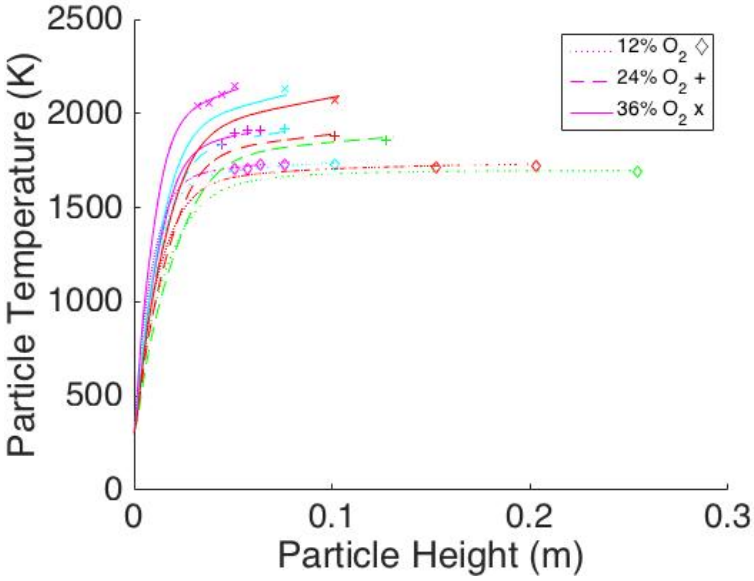

(a) Black Thunder coal

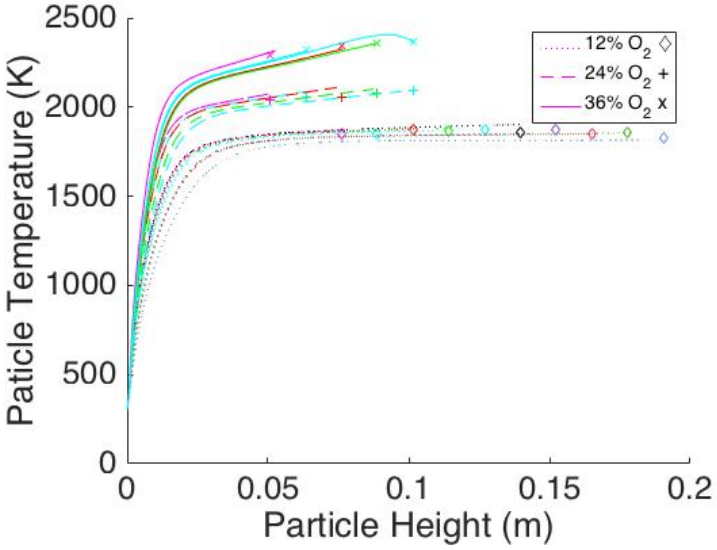

(b) North Antelope coal

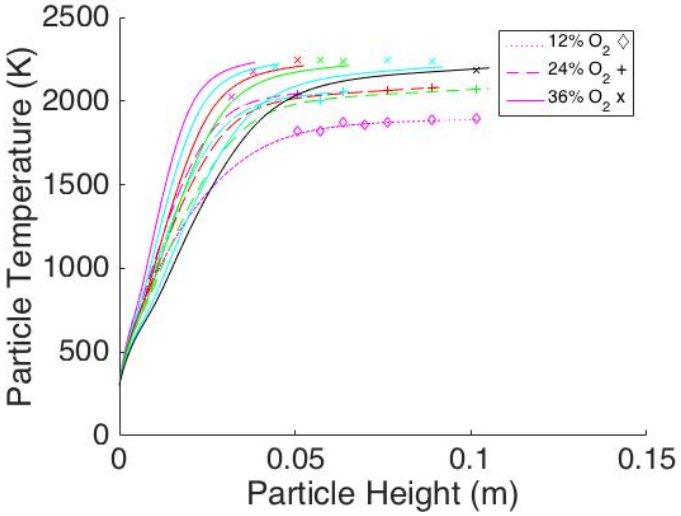

(c) Pittsburgh 8 coal

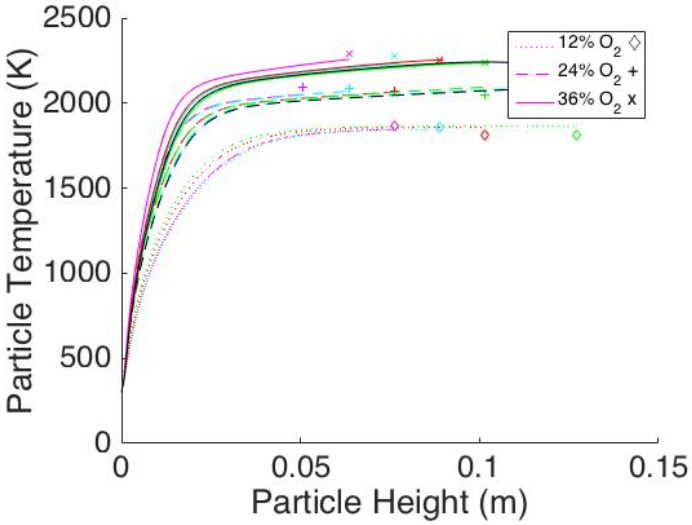

(d) Utah Skyline coal

Figure 2 – Comparison of CCK/oxy model calculations with coal data from Shaddix and coworkers[4, 5] using the measured particle diameters.

Table 12 - Difference between Calculations with Multiple Diameter Profile and Measured Particle Temperatures

Black Thunder	Mean Absolute Error (K)	Max Error (K)	Pittsburgh 8	Mean Absolute Error (K)	Max Error (K)
12 % O_2	9	14	12 % O_2	11	22
24 % O_2	16	26	24 % O_2	9	37
36 % O_2	18	40	36 % O_2	49	157
North Antelope			**Utah Skyline**		
12 % O_2	13	43	12 % O_2	33	48
24 % O_2	28	52	24 % O_2	41	81
36 % O_2	13	27	36 % O_2	17	44

4.3. Late Burnout

It should be noted that the Pittsburgh 8 data also included a selection of data points at far higher observation heights than any of the other data. Predicting the relevant diameters would have been an extreme extrapolation, so they were excluded from the optimization, but they are shown below in Figure 3 and Table 13 (a discussion of relevant kinetics follows in the next section).

Initial diameter values were selected such that CCK/oxy to precisely predict the measured mean particle temperature (upper and lower particle diameter bounds were also plotted for reference). These diameters were not selected on any basis other than that they fit the measured mean particle temperature at a given height. The diameters required to match the temperature data are uniformly unfeasible for such late burnout given the rest of the data, but this is in fact exactly what would be expected. The particles that survive to late burnout are either exceptionally persistent or they are in a near-extinction regime or near-burnout as discussed by Sun and Hurt.[19] In the case of the persistent particle, they are likely larger particles that have a particular ash content and/or maceral character that requires a longer residence time to consume. In the case of near-extinction or burnout, the particles have experienced a very significant and rapid transition to a nearly inert particle that is heated almost entirely by ambient conditions (rather

than exothermic oxidation). CCK/oxy predicts both states, and it is seen in the rapid decrease of the temperature profile (corresponding to roughly the last 15% of burnout), followed by a long, slow decline in particle temperature.[‡] Because the transition between burning and near-extinction is quite rapid, and the particles are far from uniform in their burning characteristics, it is quite unlikely that the observation height would happen to be appropriate to observe a significant number of particles mid-transition. Instead, the observations are an average of particles that are just barely hot enough to be detected, and particles that continue to burn. This average is weighted by the proportion of particles that are near burnout vs. those still burning rapidly, and that weight shifts (as expected) toward near-burnout for progressively longer residence times. Also as expected, this shift is more rapid for more intense O_2 environments. In short, the Pittsburgh 8 late burnout data support the validity of the kinetic optimization done on earlier burnout data, and all but one of the particles fall within an appropriate diameter window (as determined by the reference diameter sizes) and show a reasonable weighted average.

The largest disagreement between the model and the data in Figure 3 is the last point in the 36% O_2 environment. No diameter input into CCK/oxy, no matter how small, intersects that point, indicating that it is essentially completely converted, and the relevant energy balance is that of an inert particle. This in turn means that the kinetic submodel (and all other submodels) in CCK/oxy are no longer relevant to that particle. Instead only the energy balance is relevant, and no set of coal-specific inputs into CCK/oxy allow it to intersect the point in question, which leaves two potential conclusions: 1) Some of the standard energy balance assumptions are incorrect in this case (true, but probably not significant), or 2)

[‡] The slow decline is due largely to the continual decrease in ambient gas temperature with height in the particular experimental setup.

the gas temperature profile and/or environmental wall temperature profile are slightly incorrect (also true in some degree, and more significant).

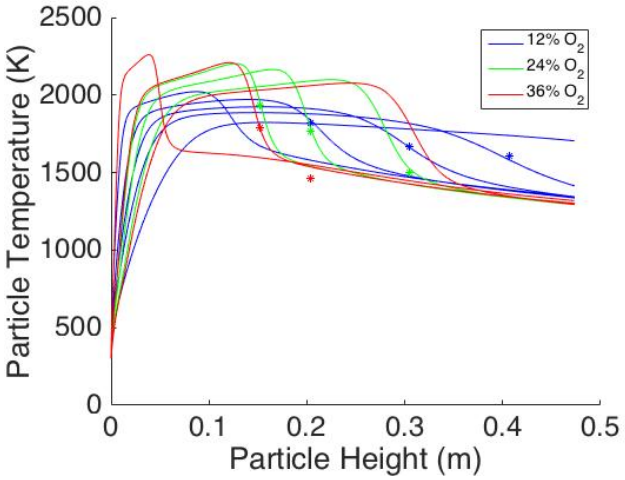

Figure 3 – Comparison of CCK/oxy model calculations with late burnout Pittsburgh 8 coal data from Shaddix and coworkers[4, 5] using the measured particle diameters.

Table 13 - Diameter Values That Match Late Burnout Predictions of Particle Temperature

Diameter Designation	12% O_2	24% O_2	36% O_2
Lower Diameter Bound (μm)	60	60	60
Diameter Match (μm)	77	93	91
Diameter Match (μm)	89	104	
Diameter Match (μm)	100		
Upper Diameter Bound (μm)	125	120	125

4.4. Kinetic Parameter Results

The optimized values of the kinetic parameters for this data set are given in Table 14. These values represent a local minimum in the kinetic parameter space, and are not unique values. This is expected and in fact unavoidable in any skeletal reaction mechanism because each reaction (R1-R8) represents an

umbrella reaction for an enormous number of similar reactions involving the complex carbon chemistry of the char, and the kinetic parameters therefore have little physical meaning. Even a perfectly correct, physically meaningful model will have an infinite number of feasible parameter sets located in a "valley" in parameter space because of the noise in the experimental data. In the case of highly auto-correlated parameters (such as A and E in the Arrhenius form), the "valley" in parameter space takes on a distinctive shape, and in the case of high dimensional parameter space in a model with limited physical meaning and correlated parameters, the single "valley" becomes many, exceptionally narrow, "valleys" each with a local minimum. This is the case of all but the simplest kinetic schemes, and there is no analytical solution to find either a local or absolute minimum, so optimization algorithms are used instead to find a local minimum. The location of the local minimum will depend on the initial guess value, but as long as appropriate constrains are set, the minimum of one "valley" is as valid as another. The optimization routine was executed from several different initial guess values, and generally found an equivalent "valley." In the small fraction of cases where the optimization ended in a substantially different local minima, failure was obvious from the results of the objective function, and the failed optimization was discarded.

Table 14 - Kinetic Parameters Optimizations

Parameter	Black Thunder	North Antelope	Pittsburgh 8	Utah Skyline
k_3 (mol/cm^3)	2.18×10^{10}	1.39×10^{10}	2.13×10^{8}	2.39×10^{10}
k_7 (mol/cm^3)	1.21×10^{9}	1.60×10^{9}	3.63×10^{8}	7.28×10^{9}
$E_{R,3}$ (kJ/mol)	117	117	180	130
$E_{R,7}$ (kJ/mol)	210	240	267	272

The kinetic parameters in Table 14 apportion carbon consumptions between the three reactive gases (O_2, CO_2, and H_2O) as seen in Table **15**. There are two trends of interest: first, with the exception of Pittsburgh 8, the consumption due to O_2 increases with higher O_2 concentration, which is unsurprising.

Second, and somewhat surprising, the very high levels of O_2 do not completely marginalize the conversion due to CO_2. This is likely due to the relative magnitudes of the temperature dependent exponential term in the relevant gasification and combustion Arrhenius equations. The high activation energy of the gasification reactions makes the exponential terms in the rate equation increase more rapidly with temperature than for the combustion reaction, and hence the gasification reactions stay significant at the high temperatures reached by the high O_2 concentrations.

Table 15 - Conversion Fraction due to each Reactive Gas (particle diameter of 100 microns)

O_2 Condition	**Black Thunder**			**North Antelope**			**Pittsburgh 8**			**Utah Skyline**		
	O_2	CO_2	H_2O	O_2	CO_2	H_2O	O_2	CO_2	H_2O	O_2	CO_2	H_2O
12%	0.72	0.25	0.03	0.82	0.16	0.02	0.89	0.09	0.02	0.82	0.15	0.03
24%	0.79	0.18	0.03	0.85	0.13	0.02	0.87	0.11	0.02	0.82	0.14	0.03
36%	0.83	0.15	0.03	0.86	0.11	0.02	0.87	0.11	0.03	0.85	0.12	0.04

4.5. Extrapolation from 12% O_2 Data

The literature data used here are of exceptional quality and detail, with a very wide range of O_2 concentrations and parallel experiments using both CO_2 and N_2 as the gas diluent. Unfortunately, this level of detail and O_2 range is unusual, so it is desirable to determine whether or not the CCK/oxy model is effective when extrapolating from only a single O_2 concentration, rather than the entire span of the O_2 range. The 12% case was chosen for the single condition optimization because, while it is the least informative about the effects of extreme conditions, the overwhelmingly most common literature scenario is a relatively low O_2 concentration. The following kinetic parameter optimizations were performed using the same diameter profiles shown in Table 11, but only the four data sets from the 12% O_2 environment were used. Then, the resultant kinetic parameters were used to extrapolate to the 24% and 36% O_2 conditions for their respective coals. The results are shown in Figure 4 and Table 17, while the bullet points below highlight several important points of the results:

1. Only the activation energy and preexponential factor of R3 were optimized in this case. This was done because a brief exploration of the gasification parameters showed that any reasonable set of gasification kinetic parameter values gave equivalent results at both the 12% O_2 gas composition *and* at the higher concentrations. It was observed that the optimization routine provided no significant inference regarding the gasification parameter values, because the gradient in the gasification dimensions of parameter space was close to zero for the 12% O_2 data (i.e., the gasification reaction was weak relative to the noise at low temperature conditions). While the gasification kinetic parameters are certainly important for the 24 and 36% O_2 conditions, little could be inferred about them from the 12% optimization, so they were fixed at the values found in the previous optimization.
2. Because optimizations in complex parameter spaces very often only find local minima, each kinetic parameter optimization was executed four times with significantly different initial guess vectors. The resultant values were sometimes quite different in individual optimizations of k_3 and E_3 (as expected in a complex space of many "peaks" and "valleys"), but the total rate constant and the goodness of fit (from the sum squared of error of the objective function) were in excellent agreement. The figures below were generated using one of the four sets of results (chosen at random), and the values in Table 17 are averages of the replicate results.
3. In evaluating the usefulness of the extrapolations shown below, two distinct questions must be asked, and this evaluation endeavors to answer only one of the two. First, it is of interest to know if the extrapolated curves have the correct shape and magnitude. In this case, that means: 1) are the particle predictions roughly the correct temperature, and 2) does the shape of the prediction curve follow the shape of the data. The second question of interest determines how well the time axis from data corresponds to the extrapolated predictions. It is necessary to decouple these two

questions because even a very small shift in the time axis can cause a large shift in temperature for very early or very late particle burnout, which gives extremely misleading results. For example, the first data point of the Black Thunder coal in the 36% O_2 extrapolation is offset from the data by approximately 2 milliseconds, which results in an error between prediction and data of roughly 160 K, which far exceeds any of the other error values in the extrapolation. Furthermore, that two milliseconds of time disappear with a slight shift of diameter or gas temperature profile (well within the range of uncertainty), and the true particle temperatures span a wide range due to slight variations in maceral character, heat capacity, or particle shape.

4. A more accurate evaluation acknowledges that there is significant variation in the exact timing of initial particle heat-up and in the exact time of particle near-extinction. The small variation on the time axis is entirely within the variation of particle size and character, and the resulting large temperature change from such a small variation emphasizes the impact and importance of describing the char particles as a distribution rather than a point estimate. To accurately answer the question of prediction trends and magnitude, the first point of the Black Thunder coal and the last point in the Utah Skyline coal from the 36% O_2 environment are not included in the average error values in Table 17.
5. The North Antelope and Black Thunder temperature extrapolations were observed to consistently under-predict the data by a small amount. This is due to a slight imbalance between the gasification and combustion carbon conversion pathways. However, as described in point 1 above, other reasonable value of the gasification kinetics neither exacerbate nor correct this deficiency, so it is thought that the noise of 12% O_2 data can be better accommodated with slightly less aggressive combustion kinetics than the value suggested by the entire body of data. These less aggressive kinetics have a very small positive impact on the 12% data under

optimization simply because of random chance in a small data sample. In the extrapolation to the entire data set, this translates to a small negative impact on the rest of the data set. No immediate solution presents itself; small, uniform data samples are simply of less value that larger, more diverse samples.

6. On the whole, the results below show that the extrapolation from low O_2 concentration up to very extreme concentrations was remarkably successful, and the CCK/oxy model may be expected to function over an exceptionally wide range of conditions. This strongly implies that the submodels effectively capture the necessary physics to make CCK/oxy a powerful predictive tool. However, it must be emphasized that the data here are a relatively small sample size of only four coals, and the current results would benefit from further validation with a wider range of data. Also, it is highly desirable to collect as much data at as many conditions as possible to minimize the type of bias observed in the Black Thunder and North Antelope results.

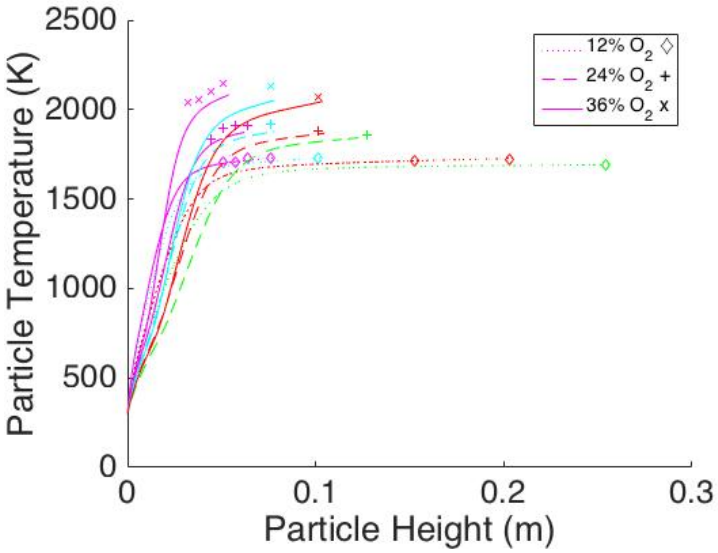

(a) Black Thunder coal

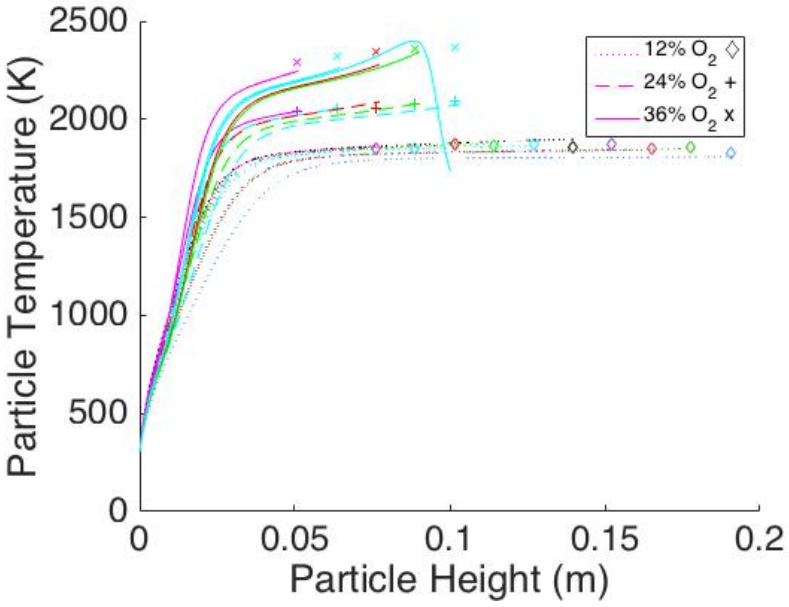

(b) North Antelope coal

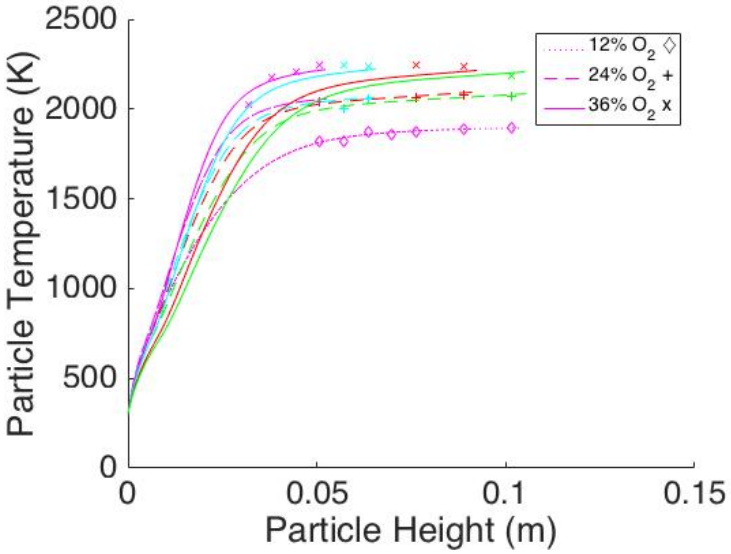

(c) Pittsburgh 8 coal

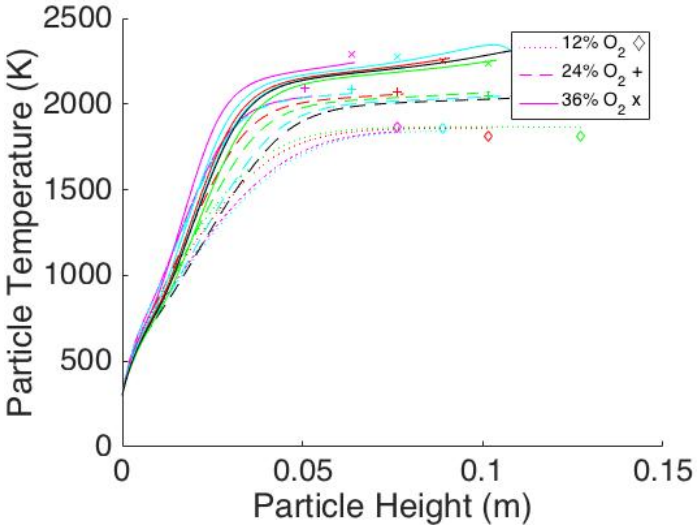

(d) Utah Skyline coal

Figure 4 –Predictions in Oxy-coal Conditions from 12% O_2 Data *Only*

Table 16 – Kinetic Parameters of the 12% O_2 Oxy-coal System

Parameter	Black Thunder	North Antelope	Pittsburgh 8	Utah Skyline
k_3 (mol/cm^3)	5.06×10^8	1.00×10^8	1.90×10^8	6.54×10^7
k_7 (mol/cm^3)	6.37×10^8	4.71×10^8	4.23×10^9	1.16×10^8
$E_{R,3}$ (kJ/mol)	178	180	180	180

Table 17 - Absolute Errors from an Optimization using only 12% O_2 Data in an Oxy-fuel Environment

Black Thunder	Mean Absolute Error (K)	Max Error (K)	Pittsburgh 8	Mean Absolute Error (K)	Max Error (K)
12 % O_2	5	11	12 % O_2	9	16
24 % O_2	38	58	24 % O_2	17	46
36 % O_2	69	92	36 % O_2	31	58
North Antelope			**Utah Skyline**		
12 % O_2	13	39	12 % O_2	35	53
24 % O_2	11	29	24 % O_2	31	60
36 % O_2	49	69	36 % O_2	49	89

4.6. Extrapolation from 12% N_2 Data

Because oxy-coal combustion has only become a popular research topic relatively recently, most literature data are not only obtained over a relatively narrow (and low) O_2 range, but are also almost always in a conventional regime using N_2 as the diluent. The CCK/oxy model would therefore be of most use if it could reasonably be calibrated from data collected at conventional conditions. Fortunately, the literature oxy-coal data used here were collected in parallel with data of the same coals at the same O_2 concentration. The two experimental conditions differed only in that the second set of experiments used N_2 as the diluent. In general, the method outlined in Section 4.5 applies to the optimizations that resulted in Figure 5 and Table 19 but differences and important similarities are highlighted below: The optimizations in this section were carried out using N_2 data and conditions as inputs to the CCK/oxy model, but the plots and tables are extrapolations that took the kinetic parameters obtained from the 12% N_2 data optimizations, and applied them to all three O_2 conditions in the oxy-fuel environment.

1. Table 18 shows the diameter values relevant to this set of experiments.
2. As in bullet point 2 in Section 4.5, four replicate optimizations were run for each set of data, and all had excellent agreement with each other except for of one of the Utah Skyline replicates. This exception found a local minimum substantially farther from the minima found by the other three replicates (i.e., the optimization routine failed to find a reasonable optimum in one instance), and the results from the exception were discarded.
3. The Pittsburgh coal data were unique in that the particle temperatures in N_2 diluent were actually substantially lower than the particle temperatures in CO_2 diluent. This one data set is inconsistent with theory, past experience, and all of the other 23 experimental data sets referenced here. The author of the paper containing the inconsistent Pittsburgh coal data theorized that this was

because the gas temperature profile (which cannot be perfectly regulated) was colder in the N_2 environment than in the CO_2 environment[4]. This is true, but even when accounting for the difference in profile temperature, the particles in the N_2 environment are predicted to be roughly 50 K hotter than the CO_2 environment, due to slower O_2 diffusion and an endothermic gasification reaction in the CO_2 environment. In the N_2 environment data, the particles were roughly 150 K *colder* than in the CO_2 environment for Pittsburgh coal. Adding in the prediction that they should be 50 K hotter, the total discrepancy is on the order of 200 K. Lacking a reasonable explanation for these anomalous data, the Pittsburgh coal data from the N_2 experiment are not shown here.

4. As before, the first point of the Black Thunder data and the last point of the North Antelope data are slightly off-set in time, and not included in the averages for Table 19.
5. The Black Thunder and North Antelope coals have the same bias towards under-prediction of the particle temperature as before, and are in general quite similar to the predictions from the extrapolations based on the 12% O_2 in oxy-fuel conditions. This implies that there is no significant reaction O_2-char reaction mechanism change between oxy-coal and conventionally fired coal.
6. The N_2 Utah Skyline coal results did not extrapolate well to the oxy-fuel data, which could indicate either: 1) that there *is* a mechanism change between the oxy-coal and conventional environments, 2) the N_2 Utah Skyline data are erroneous, or 3) that the exceptionally small N_2 Utah Skyline data set (only 3 data collection heights) is insufficient to accurately capture the combustion kinetics. The last point (option 3) is thought to be the most likely explanation.

7. As a whole, the extrapolation from conventional data at low O_2 concentrations to the full range of oxy-fuel data has some promise, but is far from conclusive. Further validation (additional data) is needed.

Table 18 – Diameter Profiles for N_2 Experiments

Coal Type O_2 % Height (cm)	Black Thunder 12 Diameter (µm)	North Antelope 12 Diameter(µm)	Utah Skyline 12 Diameter (µm)
4.45	100		
5.08	100		
5.72	100		
6.35	100	94	
7.62	100	98	102
8.89		96	99
10.16		92	99
11.43		94	
12.70	110	97	

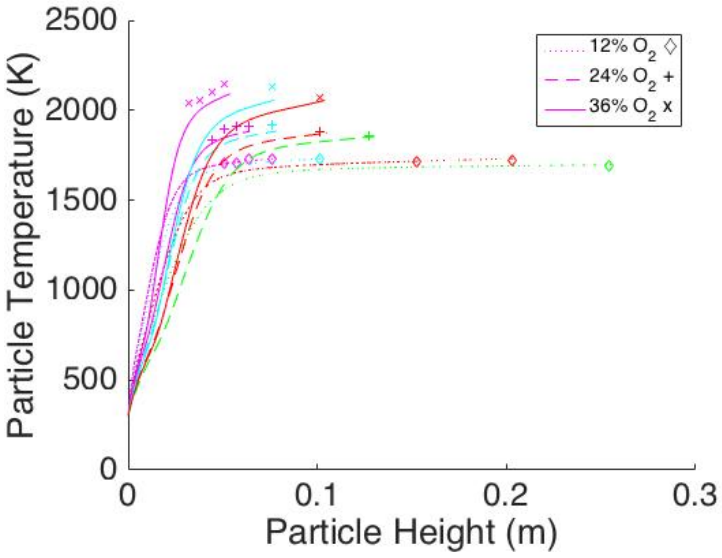

(a) Black Thunder coal

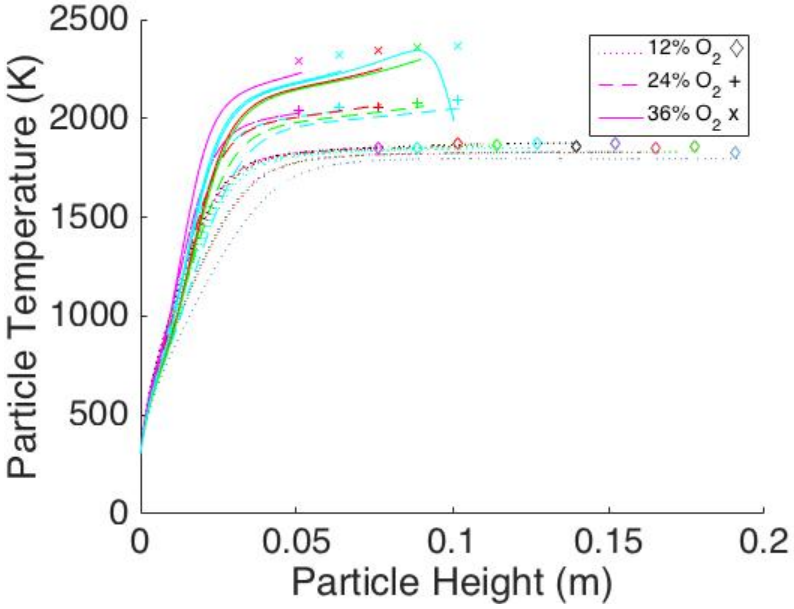

(b) North Antelope coal

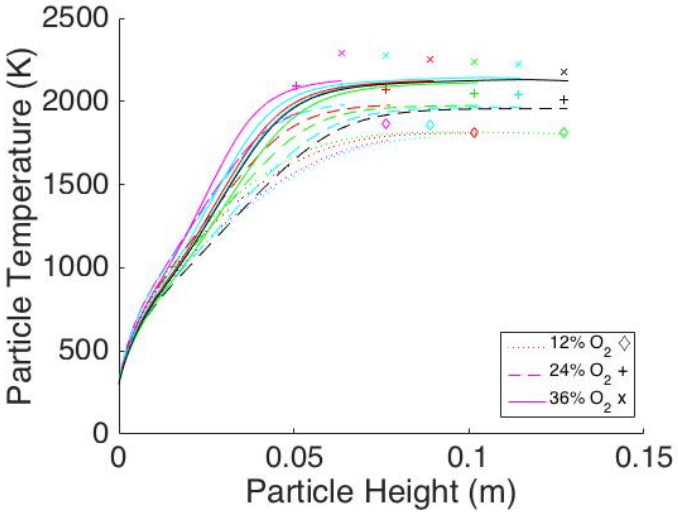

(c) Utah Skyline coal

Figure 5 –Predictions in Conventional Conditions from 12% O_2 Data Only

Table 19 - Absolute Errors from an Optimization using only 12% O2 Data in a Conventional Coal Environment

Black Thunder	Mean Absolute Error (K)	Max Error (K)	Pittsburgh 8	Mean Absolute Error (K)	Max Error (K)
12 % O_2	5	15	12 % O_2	N/A	N/A

24 % O_2	31	50	24 % O_2	N/A	N/A
36 % O_2	57	84	36 % O_2	N/A	N/A
North Antelope			**Utah Skyline**		
12 % O_2	19	44	12 % O_2	55	114
24 % O_2	19	43	24 % O_2	109	190
36 % O_2	83	102	36 % O_2	135	181

Table 20 – Kinetic Parameters for the 12% O_2 Condition in Conventional Air-fired Regime

Parameter	Black Thunder	North Antelope	Pittsburgh 8	Utah Skyline
k_3 (mol/cm^3)	1.00×10^8	1.00×10^8	N/A	2.21×10^6
k_7 (mol/cm^3)	2.20×10^9	1.00×10^8	N/A	9.41×10^6
$E_{R,3}$ (kJ/mol)	175	180	N/A	179

5. Application to CFD simulations

The literature data and the results of fitting the CCK/oxy model to data imply that a CFD simulation should take into account two distributions to accurately capture coal char particles. The first distribution is the diameter distribution of the raw coal particles that form the char. The diameter heavily impacts burnout predictions, and the mean, variance, and distribution form may propagate that impact on to the CFD simulation. In general, pulverized coal particle diameter distributions follow a Rosin-Rammler distribution, and it is this distribution that should be used in simulating industrial pulverized coal systems. For the experimental literature data used here, the full distribution is expected to be approximately normal after sieving, swelling, and fragmentation, but the observed data are likely to be a truncated normal distribution. This is because the small diameter and/or rapidly oxidizable portion of the distribution quickly becomes undetectable due to the small radiative emission from these particles. The exact truncation point in the normal diameter distribution is unknown, and it is not consistent between burner heights, coal type, or O_2 condition. To fully describe the true distribution of a data set, a correlation between particle detectability, temperature, and diameter would be devised. Accurate

parameters for such a correlation would assume a char emissivity, require an assumed distribution for the raw coal, and incorporate knowledge of the optical limits of the detecting system. These assumptions, in conjunction with the coal swelling model, would predict the post-devolatilization diameter of a char particle, and the partially burned diameter at a given height, and appropriate correlation parameters would reconstruct the entire raw coal input diameter distribution.

The second distribution of interest is the change in particle combustion behavior due to maceral character and ash content. For a given particle diameter, the combustion temperatures (from the literature data referenced in this work) vary by approximately ±150 K. If these values are simply used as error bars, the high accuracy of the CCK/oxy model is effectively useless. Instead, this variation should not be treated as error, but as actual variation in any given cohort of particles. The data shown here imply that a normal distribution with a mean of the CCK/oxy temperature prediction and a variance of approximately 75 K may be appropriate to capture the particle-to-particle variation.

An appropriate CFD application to combine accuracy and computational efficiency is needed. One potential method would be to first determine the initial particle diameter distribution. Given an approximation of that distribution, CCK/oxy can be executed using “n” diameters that cover the distribution in sufficient detail. Bin values separated by 10 microns are likely adequate. For each bin, CCK/oxy should be executed with a gamut of gas temperature and composition profiles, and the output vectors recorded. Finally, the output vectors for a given bin size would be used to train a surrogate function that depends on gas composition, temperature, and the peak temperature in the burnout history of the particle. Such a function would execute very rapidly but potentially capture the majority of the information of the CCK/oxy model. Implementation into a CFD simulation would appropriately weight the available particle diameters and temperature variation within each diameter according to the two distributions described above.

6. Conclusions

A comprehensive coal char conversion model (Carbon Conversion Kinetics) was extended to function at the extremes of oxy-coal combustion environments. These extensions included both numerical stability and submodel accuracy, including improved submodels for coal devolatilization, the mode of burning parameter, coal particle swelling, and the thermal annealing model. These improvements are thought to be valid in any char combustion regime, rather than being limited to oxy-coal combustion specifically. The specific submodel improvements given here were previously indicated to be the most sensitive submodels in a comprehensive, global sensitivity analysis.[7] Model improvements were implemented and the model was subsequently validated and explored by optimizing the model oxidation and gasification parameters to match a selection of the highly limited oxy-coal data from the literature. The validation revealed:

1. The CCK/oxy model matched the available data extremely well, with enormous improvement over past attempts using the CCK model.[7, 8] The CCK/oxy model was able to simultaneously fit all O_2 conditions for a given coal with a single set of kinetic parameters. This was largely due to improvements in the devolatilization, swelling, and mode of burning models, as well as more exacting numerical solutions. The thermal annealing model is also exceptionally sensitive, but it is so tightly coupled to the kinetic preexponential factor that the submodel has minimal impact when optimizing the kinetic parameters of a single coal in a narrow range of heating rates and peak temperatures. Instead, the annealing model is vitally important to any attempt to create coal-general kinetic correlations or in exploring widely varying heating rate and peak temperature regimes with a given coal.
2. The CCK/oxy model, when optimized to the 12% O_2 oxy-coal data **only**, made reasonable extrapolations to 24 and 36% O_2 conditions.

3. The CCK/oxy model, when optimized to the 12% O_2 conventional fired condition, made reasonable extrapolations to all levels of oxy-coal firing in two of three cases. These results are inconclusive, but imply that data collected in conventional firing conditions may be useful in determining kinetic parameters relevant to oxy-coal scenarios.
4. In oxy-fuel conditions, several competing effects complicate the combustion regime. These effects are mainly due to high concentrations of gasification reactants (especially CO_2), high temperatures that accompany enhanced O_2 levels, and a balance between endothermic and exothermic reactions. The CCK/oxy model predictions are as anticipated: 1) that O_2 combustion is by far the dominant reaction pathway, 2) that gasification becomes relatively less important at more intense oxygen conditions, and 3) that gasification becomes relatively more important at high temperature. The last two effects are in competition, and the second effect proved dominant here.

Finally, as the present work was intended to support predictive boiler design via computational fluid dynamics simulation, a brief suggestion for CFD application was outlined. In this work, it was observed that both particle diameter distributions and particle reactivity distributions are vitally important to accurate model predictions. As CFD work ideally models the entirety of both distributions, accurate descriptions of both distributions must be estimated as closely as possible. This estimation is problematic when data are collected via radiant particle detection, because certain subsections of the activity and size distribution fall below the lower temperature and size limit of detectability.

Acknowledgements

This material is based upon work supported by the Department of Energy, National Nuclear Security Administration, under Award Number DE-NA0002375.

Funding for this work was also provided by the Department of Energy through the Carbon Capture Simulation Initiative. This report was prepared as an account of work sponsored by an agency of the United States Government. Neither the United States Government nor any agency thereof, nor any of their employees, makes any warranty, express or implied, or assumes any legal liability or responsibility for the accuracy, completeness, or usefulness of any information, apparatus, product, or process disclosed, or represents that its use would not infringe privately owned rights. Reference herein to any specific commercial product, process, or service by trade name, trademark, manufacturer, or otherwise does not necessarily constitute or imply its endorsement, recommendation, or favoring by the United States Government or any agency thereof. The views and opinions of authors expressed herein do not necessarily state or reflect those of the United States Government or any agency thereof.

Release Number:

This document is authorized for public release (LA-UR-16-29489).

References

1. Wall, T.; Liu, Y. H.; Spero, C.; Elliott, L.; Khare, S.; Rathnam, R.; Zeenathal, F.; Moghtaderi, B.; Buhre, B.; Sheng, C. D.; Gupta, R.; Yamada, T.; Makino, K.; Yu, J. L., An overview on oxyfuel coal combustion-state of the art research and technology development. *Chemical Engineering Research & Design* **2009,** 87, (8A), 1003-1016.
2. Scheffknecht, G.; Al-Makhadmeh, L.; Schnell, U.; Maier, J., Oxy-fuel coal combustion-a review of the current state-of-the-art. *International Journal of Greenhouse Gas Control* **2011,** 5, S16-S35.
3. Hecht, E. S.; Shaddix, C. R.; Geier, M.; Molina, A.; Haynes, B. S., Effect of CO_2 and steam gasification reactions on the oxy-combustion of pulverized coal char. *Combustion and Flame* **2012,** 159, 3437-3447.
4. Shaddix, C. R.; Molina, A., Particle imaging of ignition and devolatilization of pulverized coal during oxy-fuel combustion. *Proceedings of the Combustion Institute* **2009,** 32, 2091-2098.
5. Geier, M.; Shaddix, C. R.; Davis, K. A.; Shim, H. S., On the use of single-film models to describe the oxy-fuel combustion of pulverized coal char. *Applied Energy* **2012,** 93, 675-679.
6. Holland, T. M.; Fletcher, T. H., Global sensitiivity analysis for a comprehensive char conversion model in oxy-fuel conditions. *Energy & Fuels* **2016,** 30, 9339−9350.
7. Holland, T. M.; Bhat, K. S.; Marcy, P.; Gattiker, J.; Kress, J. D.; Fletcher, T. H., Reduction of coal reactivity to O_2 and CO_2 due to prepartion condition dependent thermal annealing. *In Preparation* **2016**.
8. McConnel, J.; Sutherland, J., The effect of model fidelity on prediction of char burnout for single-particle coal combustion. *Proceedings of the Combustion Institute* **2017,** 36, (2), 2165-2172.
9. Holland, T. M. Computational physics of coal-fired power generation: Oxy-coal combustion and amine capture. PhD Dissertation (in progress), Chemical Engineering Department, Brigham Young University, 2017.
10. Shurtz, R. C.; Fletcher, T. H., Coal char- CO_2 gasification measurements and modeling in a pressurized flat-flame burner. *Energy & Fuels* 27, 3022-3038.
11. Hurt, R.; Sun, J. K.; Lunden, M., A kinetic model of carbon burnout in pulverized coal combustion. *Combustion and Flame* **1998,** 113, 181-197.
12. Bhatia, S. K.; Perlmutter, D. D., A random pore model for fluid-solid reactions. 1. Isothermal, kinetic control. *AIChE J* **1981,** 27, (2), 247-254.
13. Shurtz, R. C.; Kolste, K. K.; Fletcher, T. H., Coal swelling model for high heating rate pyrolysis applications. *Energy & Fuels* **2011,** 25, (5), 2163-2173.
14. McBride, B.; Zehe, M.; Gordon, S. *Nasa glenn coefficients for calculating thermodynamic properties of individual species*; John H. Glenn Research Center: Cleveland, Ohio, 2002; p 291.
15. Rowley, R. L.; Wilding, W. V.; Oscarson, J. L.; Yang, Y.; Giles, N. F., Dippr® data compilation of pure chemical properties. In *Design Institute for Physical Properties, AIChE*, Design Institute for Physical Properties, AIChE: New York, NY, 2010.
16. Haugen, N. E. L.; Mitchell, R. E.; Tilghman, M. B., A comprehensive model for char particle conversion in environments containing O_2 and CO_2. *Combustion and Flame* **2015,** 162, (4), 1455-1463.
17. Haugen, N. E. L.; Tilghman, M. B.; Mitchell, R. E., The conversion mode of a porous carbon particle during oxidation and gasification. *Combustion and Flame* **2014,** 161, (2), 612-619.
18. Skokova, K. A. Selectivity in the carbon-oxygen reaction. Pennsylvania State University, Pennsylvania, 1997.
19. Sun, J. K.; Hurt, R. H., Mechanisms of extinction and near-extinction in pulverized solid fuel combustion. *Proceedings of the Combustion Institute* **2000,** 28, 2205-2213.
20. Shurtz, R. Effects of pressure on the properties of coal char under gasification conditions at high initial heating rates. Chemical Engineering, Brigham Young University, Brigham Young University, 2011.
21. Niksa, S.; Liu, G. S.; Hurt, R. H., Coal conversion submodels for design applications at elevated pressures. Part i. Devolatilization and char oxidation. *Progress in Energy and Combustion Science* **2003,** 29, 425-477.
22. Liu, G. S.; Niksa, S., Coal conversion submodels for design applications at elevated pressures. Part ii. Char gasification. *Progress in Energy and Combustion Science* **2004,** 30, 679-717.

23. Hurt, R. H.; Calo, J. M., Semi-global intrinsic kinetics for char combustion modeling. *Combustion and Flame* **2001,** 125, 1138-1149.
24. McKay, M. D.; Beckman, R. J.; Conover, W. J., A comparison of three methonds for selecting values of input variabls in the analysis of output from a computer code. *Technometrics* **1979,** 21, (2), 239-245.
25. Fletcher, T. H.; Kerstein, A. R.; Pugmire, R. J.; Solum, M. S.; Grant, D. M., Chemical percolation model for devolatilization .3. Direct use of C-13 NMR data to predict effects of coal type. *Energy & Fuels* **1992,** 6, (4), 414-431.
26. Grant, D. M.; Pugmire, R. J.; Fletcher, T. H.; Kerstein, A. R., Chemical model of coal devolatilization using percolation lattice statistics. *Energy & Fuels* **1989,** 3, (2), 175-86.
27. Genetti, D.; Fletcher, T. H.; Pugmire, R. J., Development and application of a correlation of C-13 NMR chemical structural analyses of coal based on elemental composition and volatile matter content. *Energy & Fuels* **1999,** 13, (1), 60-68.
28. Genetti, D. An advanced model of coal devolatilization based on chemical structure. Chemical Engineering, Brigham Young University, Provo, UT, 1999.
29. Hurt, R. H.; Mitchell, R. E. In *On the combustion kinetics of heterogeneous char particle populations*, ACS Division of Fuel Chemistry, 1991; 202, pp 951-959.
30. Essenhigh, R. H., Influence of initial particle density on the reaction mode of porous carbon particles. *Combustion and Flame* **1994,** 99, (2), 269-279.
31. Smith, I. W., The combustion rates of coal chars: A review. *Symposium (International) on Combustion* **1982,** 19, 1045-1065.
32. Mitchell, R. E.; Hurt, R. H.; Baxter, L. L.; Hardesty, D. R. *Compilation of sandia coal char combustion data and kinetic analyses. Milestone report*; Sandia National Laboratories: Livermore, Ca, 1992; p 615.
33. Oh, M. S.; Peters, W. A.; Howard, J. B., An experimental and modeling study of softening coal pyrolysis. *Aiche Journal* **1989,** 35, (5), 775-792.
34. Yang, H.; Li, S.; Fletcher, T. H.; Dong, M., Simulation of the swelling of high-volatile bituminous coal during pyrolysis. *Energy & Fuels* **2014,** 28, (11), 7216-7226.
35. Yang, H.; Li, S.; Fletcher, T. H.; Dong, M., Simulation of the swelling of high-volatile bituminous coal during pyrolysis. Part 2: Influence of the maximum particle temperature. *Energy & Fuels* **2015,** 29, (6), 3953-3962.
36. Yu, J. L.; Lucas, J.; Wall, T.; Liu, G.; Sheng, C. D., Modeling the development of char structure during the rapid heating of pulverized coal. *Combustion and Flame* **2004,** 136, (4), 519-532.
37. Kidena, K.; Yamashita, T.; Akimoto, A., Prediction of thermal swelling behavior on rapid heating using basic analytical data. *Energy & Fuels* **2007,** 21, (2), 1038-1041.
38. Gale, T. K.; Bartholomew, C. H.; Fletcher, T. H., Decreases in the swelling and porosity of bituminous coals during devolatilization at high heating rates. *Combustion and Flame* **1995,** 100, (1-2), 94-100.
39. Mitchell, R. E.; R.H., H.; L.L., B.; D.R., H. *Compilation of Sandia coal char combustion data and kinetic analyses. Milestone report*; Sandia National Laboratories: Livermore, Ca, 1992; p 615.